Hindawi
Mathematical Problems in Engineering
Volume 2018, Article ID 7452863, 11 pages
https://doi.org/10.1155/2018/7452863

Research Article

Inverse Problem Solution and Regularization Parameter Selection for Current Distribution Reconstruction in Switching Arcs by Inverting Magnetic Fields

Jinlong Dong, Guogang Zhang, Zhiqiang Zhang, Yingsan Geng, and Jianhua Wang

State Key Lab of Electrical Insulation and Power Equipment, School of Electrical Engineering, Xi'an Jiaotong University, Xi'an, Shaanxi 710049, China

Correspondence should be addressed to Guogang Zhang; ggzhang@mail.xjtu.edu.cn

Received 8 February 2017; Accepted 14 November 2017; Published 4 January 2018

Academic Editor: Salvatore Alfonzetti

Current density distribution in electric arcs inside low voltage circuit breakers is a crucial parameter for us to understand the complex physical behavior during the arcing process. In this paper, we investigate the inverse problem of reconstructing the current density distribution in arcs by inverting the magnetic fields. A simplified 2D arc chamber is considered. The aim of this paper is the computational side of the regularization method, regularization parameter selection strategies, and the estimation of systematic error. To address the ill-posedness of the inverse problem, Tikhonov regularization is analyzed, with the regularization parameter chosen by Morozov's discrepancy principle, the L-curve, the generalized cross-validation, and the quasi-optimality criteria. The provided range of regularization parameter selection strategies is much wider than in the previous works. Effects of several features on the performance of these criteria have been investigated, including the signal-to-noise ratio, dimension of measurement space, and the measurement distance. The numerical simulations show that the generalized cross-validation and quasi-optimality criteria provide a more satisfactory performance on the robustness and accuracy. Moreover, an optimal measurement distance can be expected when using a planner sensor array to perform magnetic measurements.

1. Introduction

Low voltage circuit breakers (LVCBs) are widely used in power distribution systems to protect people and electrical equipment against a fault current. LVCBs are characterized by electric arcs, which are hot and conductive plasmas. The current distribution in electric arcs is an essential parameter that determines the distribution of heat flux and temperature, the erosion ratio of electrodes, and the interaction of arcs with surroundings [1, 2]. A better knowledge of it helps to understand the complex physical behavior of electric arc plasmas.

This paper is focused on the reconstruction of current density distribution inside LVCBs by employing an inverse problem technique. This technique is concerned with the solution of a linear magnetic inverse problem of reconstructing the internal current profiles from the measurements of magnetic fields [3]. A large wealth of applications can be addressed by this technique and has provided many interesting results in different fields [4–7].

In [8], the average arc positions, shapes, and arc dynamics are obtained from the magnetic measurements, by assuming electrical arcs and conductors in LVCBs to be a succession of 2D rectilinear and thread-like elements of current. But the result is not sufficient to obtain the current distribution. Reference [9] is focused on current density reconstruction in vacuum arcs inside high voltage vacuum circuit breakers, using the inverse problem technique. Several regularization techniques have been studied to address the ill-posedness of the inverse problem. But the spatial resolution is intrinsically poor and is merely to allow spotting the position of the arc core and its macroscopic shape. In our previous work [10], we reported that a 2D current density distribution can be reconstructed by inverting only one component of the magnetic field. The Morozov discrepancy principle is used as

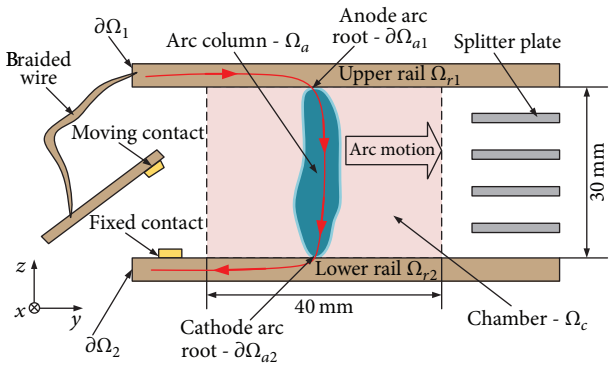

FIGURE 1: Geometry of a typical LVCB model.

the parameter selector owing to the prior knowledge of noise level in measurements. In [11], we are focused on the impact of nonidealities of magnetic sensors in the current distribution reconstruction in switching air arcs. The application is relevant and the modeling of sensor nonidealities in sensors systems is a keypoint.

However, an essential problem, that must be tackled urgently, is how to choose the regularization parameter automatically or the parameter selection criteria in regularizing procedures, especially, when there is nothing known about the exact solution and the noise level. Another important issue is that using the magnetic field component makes the inverse problem more ill-posed. Thus, there is a need for us to pay more attention to the regularization procedure and its parameter selection.

This paper expands the analysis of [10] to study the magnetic inverse problem of reconstructing a 2D current distribution in LVCBs. We explore the performance of four common-used parameter selectors, namely, the discrepancy principle, the L-curve, generalized cross-validation, and quasi-optimality criteria, complemented by Tikhonov regularization to address the ill-posedness. Effects of several features on the performance of these selectors have been investigated, such as the signal-to-noise ratio, dimension of measurement space, and measurement distances. The objective of this paper is the computational side of the regularization method, regularization parameter selection strategies, and the estimation of systematic error.

2. Mathematical Methods for Forward Modeling

A simplified and generally used geometry of LVCB with two parallel arc runners is proposed as shown in Figure 1. Similar geometries can be found in various studies in [2, 12, 13]. In general, when the LVCB interrupts a fault current, an electric arc is ignited between the contacts. The arcing process can be divided into three phases: arc ignition between two contacts, arc motion in the chamber, and arc splitting [2]. The splitter plates are usually made of ferromagnetic materials, such as steel, which leads to a nonlinear and complex magnetic phenomenon, especially, during the arc splitting phase.

To simplify the problem, this work is focused on the second phase when the arc is moving between the parallel rails in the chamber. During this phase, the current is flowing through the upper rail, the arc, and finally the lower rail. Nonlinear effects of splitters are assumed to be negligible considering that the arc column is far away from nonlinear ferromagnetic plates in this phase [14]. Thus, the reconstruction of arc current distribution can be modeled by a linear magnetic inverse problem. Generally, the dimension of the arc and other conductors in LVCBs along x-axis is much smaller than that along y-axis and z-axis and thus, the 2D case is investigated in this study.

2.1. Forward Modeling. We confine the 2D problem of current density distribution reconstruction to the chamber domain Ω_c for the second phase, where $\Omega_c := \{(x, y, z) \in R^3 \mid x = 0,\ 0 \le y \le 40\,\text{mm},\ 0 \le z \le 30\,\text{mm}\}$. The upper and lower rails are 40 mm long (y-axis) and 2 mm wide (z-axis) located on the upper and lower side of the chamber domain, respectively. Other conductors, such as current fed-in wires, are not taken into consideration.

We assume a magnetostatic condition over the exterior with a sufficiently smooth boundary $\Omega_e := \mathbb{R}^3 \setminus \overline{\Omega}_c$, and no ferromagnetic material inclusions over Ω_c and Ω_e. The magnetostatic approximation is common to computational approaches for the multi-physical simulation of electric arcs [14, 15]. The rails are made of copper. Then the forward problem, that is, calculation of the magnetic field from the current density distribution, can be introduced by the Biot-Savart law

$$H(r) = \int_\Omega J(r_S) \times \Phi(r_S, r)\, d\Omega,$$
$$\Phi(r_S, r) = \frac{1}{4\pi} \frac{r - r_S}{|r - r_S|^3},\quad r_S \in \Omega,\ r \in \Omega_e, \tag{1}$$

where J is a continuous current density distribution over source domain $\Omega := \Omega_c \cup \Omega_{r1} \cup \Omega_{r2}$, $H := (H_x, H_y, H_z)$ the magnetic field over Ω_e, $r_S := (0, y_s, z_s)$ the integration point, and $r := (x, y, z)$ the measurement point. In general, for the forward problem of (1), Ω_a and its boundaries are not known accurately but are determined to be bounded within the already given chamber domain Ω_c, so we have $\Omega_a \subset \Omega_c$ and the current vanishes over the nonarcing area $\Omega_c \setminus \Omega_a$.

Let I be the total current flowing through the LVCB, which is supposed to be known. The boundary $\partial\Omega_1$ (resp., $\partial\Omega_2$) is where the current enters (resp., leaves) the LVCB, and $\partial\Omega_0$ is the rest of boundaries with no cross flows of current. Boundary conditions (BCs) of the model are given by

$$\int_{\partial\Omega_i} J \cdot n_i\, dS = I_i,\quad i \in \{0, 1, 2\}, \tag{2}$$

where n_i denotes the outward normal unit vector of $\partial\Omega_i$ and I_0 (resp., I_1, I_2) is equal to 0 (resp., $+I$, $-I$).

2.2. Measurement Model. Magnetic measurements are carried out by some hypothetical magnetic sensors along x-axis. In this direction, the upper rail (Ω_{r1}), the lower rail (Ω_{r2}),

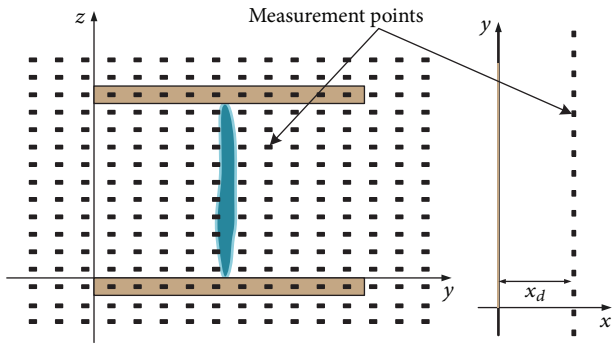

Figure 2: Set-up of measurement points.

and the electric arc (Ω_a) provide magnetic contributions, respectively, $H_{r1}(x)$, $H_{r2}(x)$, and $H_a(x)$. The total magnetic field components along x-axis is given by

$$H(x) = H_{r1}(x) + H_{r2}(x) + H_a(x). \tag{3}$$

The measurement points are uniformly distributed on a plane. The plane is placed outside the chamber as shown in Figure 2. Precisely, let Γ be the measurement plane with a distance of x_d (x-axis) from the chamber, where $\Gamma := \{(x, y, z) \in R^3 \mid x = x_d,\ -20\,\text{mm} \le y \le 60\,\text{mm},\ -15\,\text{mm} \le z \le 45\,\text{mm}\}$. Let P_y be a set of points uniformly distributed over y-direction and P_z a set of points uniformly distributed over z-direction. Then the hypothetical magnetic sensors are positioned at the point matrix $P := P_y \times P_z$. The total number of measurement points is denoted by $m := |P|$. We assume that magnetic field components are returned with a high enough temporal resolution.

From (3), it shows that the measurement is a composition of magnetic contributions by both the arc and rails. Noting that the geometry and material properties of rails are well known but those of the electric arc are not, the current density distribution J_{r1} over Ω_{r1} (upper rail) and J_{r2} over Ω_{r2} (upper rail) can be computed by solving a conduction problem. In this work, J_a over Ω_a (arc column) is intended to be reconstructed with the inverse problem technique. Thus, to simplify the mathematical computation, we assume that arc roots have been obtained by some experimental methods [8, 16, 17]; that is, arc roots locations ($\partial\Omega_{a1}$ and $\partial\Omega_{a2}$) are given. Boundary conditions on arc roots are given by

$$\int_{\partial\Omega_{ai}} J \cdot n_i \, dS = I_i, \quad i \in \{1, 2\}, \tag{4}$$

where I_1 (resp., I_2) is equal to $+I$ (resp., $-I$).

With this assumption, magnetic contributions ($H_{r1}(x)$ and $H_{r2}(x)$) of all the other conductors in the model can be calculated by solving the conduction problem supplemented by BCs of (2) and (3) and then eliminated from the measurement data; that is, the magnetic field $H_a(x)$ only produced by the arc is returned. We collect $H_a(x)$ into the measurement vector $\mathbf{H} = [H_{a1}, H_{a2}, \ldots, H_{am}]^T$ and $\mathbf{H} \in \mathbb{R}^m$.

2.3. Model Discretization Method. The finite integration technique (FIT) [18] is used for the discretization of the chamber domain, which assumes a network of wires as an approximation to the continuous domain. We employ a discretization with levels n_y, n_z in the direction of the y- and z-axis, respectively. Each wire is assumed to coincide with an edge of l_j with its orientation denoted by $\mathbf{e}_j$, where $\mathbf{e}_j := [0, 1, 0]^T$ if l_j is parallel to the y-axis or $\mathbf{e}_j := [0, 0, 1]^T$ if it is parallel to the z-axis. The magnitude of the current flowing through l_j is denoted by J_j. Discretized currents are collected into the vector $\mathbf{J} := [J_1, J_2, \ldots, J_n]^T$ and $\mathbf{J} \in \mathbb{R}^n$ with parameter n of total unknowns. Thus, the degrees of freedom are the current amplitude in each wire.

For the discretization of the Biot-Savart integral operator, the straightforward rectangular rule is used for the calculation of the integrals in (1), which leads to linear convergence for the forward problem. For the calculation of the Biot-Savart integrals for each edge l_j and edge current J_j, we employ an exact integration of the magnetic field for a straight wire as explicitly given by equation (5.64) in [19]; that is,

$$\begin{pmatrix} \Lambda_{ij}(x) \\ \Lambda_{ij}(y) \\ \Lambda_{ij}(z) \end{pmatrix} = \frac{1}{4\pi} \int_{l_j} \frac{\mathbf{e}_j \times (x_i - x_s, y_i - y_s, z_i - z_s)^T}{\left((x_i - x_s)^2 + (y_i - y_s)^2 + (z_i - z_s)^2\right)^{3/2}} dl_j, \tag{5}$$

where $r_i := (x_i, y_i, z_i)$ is the ith measurement point and $r_S := (x_s, y_s, z_s) \in l_j$ is the integration point.

Thus we introduce the finite dimensional discrete analogue of Biot-Savart operator $\mathbf{W} \in \mathbb{R}^{m \times n}$, where $\mathbf{W}_{ij} = \Lambda_{ij}(x)$ and the forward problem is transformed into a matrix operator form as

$$\mathbf{WJ} = \mathbf{H}. \tag{6}$$

3. The Inverse Problem

3.1. Tikhonov Regularization Approach. The magnetic inverse problem is to find the unknown current density distribution from the magnetic field by solving a linear integral equation of the first kind, that is, solving (1), or by solving its discrete form, that is, solving (6). It is well known from functional analysis that the Biot-Savart operator $\mathbf{W}$ is a linear, bounded, and compact operator from $(L^2(\Omega_c))^3$ to $(L^2(\Omega_e))^3$ with exponentially decaying singular values and can not be continuously invertible [20]. This leads to highly unstable reconstructions where small measurement errors in the right hand side of (6) can cause strong perturbations in the solution; that is, the inverse problem of (6) is seriously ill-posed.

Therefore, it is necessary to employ regularization methods to make the ill-posed problem more regular in order to stabilize the problem and to single out a useful and stable solution, that is, to approximate the unbounded operator pseudoinverse $\mathbf{W}^{-1}$ by a bounded and stable operator $\mathbf{R}_\alpha$

with regularization parameter $\alpha \geq 0$. We employ Tikhonov regularization to yield a least squares solution defined as

$$\mathbf{J}_{\text{reg}} = \arg\min_{J\in\mathbb{R}^n} \left\{ \|\mathbf{WJ} - \mathbf{H}\|_2^2 + \alpha^2 \left\|\mathbf{L}\left(\mathbf{J} - \mathbf{J}_0\right)\right\|_2^2 \right\}, \quad (7)$$

where matrix $\mathbf{L}$ is typically either the identity matrix $\mathbf{I}_n$ or a $p \times n$ discrete approximation of the $(n - p)$th derivative operator, in which case $\mathbf{L}$ is a banded matrix with full row rank. An initial guess $\mathbf{J}_0$ of the solution is included in the side constraint. Thus, the regularization strategy is defined by

$$\mathbf{R}_\alpha = \left(\alpha^2 \mathbf{L}^* \mathbf{L} + \mathbf{W}^* \mathbf{W}\right)^{-1} \mathbf{W}^* \quad \text{with } \|\mathbf{R}_\alpha\|_2 \leq \frac{1}{2\sqrt{\alpha}}, \quad (8)$$

where $\mathbf{W}^*$ is the complex conjugate transpose matrix of $\mathbf{W}$.

We estimate the error for the reconstruction of current density distribution from

$$\mathbf{J}_{\text{reg}}^{(\delta)} = \mathbf{R}_\alpha \mathbf{H}^{(\delta)} \quad \text{with } \left\|\mathbf{H}^{(\delta)} - \mathbf{H}\right\|_2 \leq \delta \quad (9)$$

by

$$\begin{aligned} \left\|\mathbf{J}_{\text{reg}}^{(\delta)} - \mathbf{J}\right\|_2 &= \left\|\mathbf{R}_\alpha \mathbf{H}^{(\delta)} - \mathbf{R}_\alpha \mathbf{H} + \mathbf{R}_\alpha \mathbf{H} - \mathbf{J}\right\|_2 \\ &\leq \left\|\mathbf{R}_\alpha \mathbf{H}^{(\delta)} - \mathbf{R}_\alpha \mathbf{H}\right\|_2 + \left\|\mathbf{R}_\alpha \mathbf{WJ} - \mathbf{J}\right\|_2 \\ &\leq \left\|\mathbf{R}_\alpha\right\|_2 \delta + \left\|\mathbf{R}_\alpha \mathbf{WJ} - \mathbf{J}\right\|_2, \end{aligned} \quad (10)$$

where $\mathbf{H}^{(\delta)} := \mathbf{H} + \boldsymbol{\delta}$ is the perturbed measurement of magnetic field, $\boldsymbol{\delta}$ the measurement error, and $\mathbf{J}_{\text{reg}}^{(\delta)}$ the regularized solution of $\mathbf{J}$ from $\mathbf{H}^{(\delta)}$. The first term on the right hand side of (10), called perturbation error, describes the error coming from the data noise of $\delta = \|\boldsymbol{\delta}\|_2$ multiplied by the approximation $\mathbf{R}_\alpha$. The second term, called regularization error, denotes the approximation error $\|(\mathbf{R}_\alpha - \mathbf{W}^{-1})\mathbf{J}\|_2$ which purely depends on $\mathbf{R}_\alpha$ and is irrelevant to the measurement error $\boldsymbol{\delta}$. Usually, the first term tends to infinity for $\alpha \to 0$ while the second term tends to zero with a pointwise convergence.

3.2. Regularization Parameters Selection. The regularization parameter controls the weight given to minimization of the perturbation error relative to minimization of the regularization and also controls the sensitivity of the regularized solution $\mathbf{J}_{\text{reg}}^{(\delta)}$ to perturbations in $\mathbf{W}$ and $\mathbf{H}$. Thus, the strategy to choose $\alpha = \alpha(\delta)$ dependent on δ is an essential issue to ensure a stable and reliable regularized solution by keeping the total error as small as possible; that is, we would like to minimize the right hand side in (10).

In this work, four common criteria for the choice of the regularization parameter α are studied depending on the assumption about the 2-norm of the perturbation δ.

For the case where a good estimate of δ is known, Morozov's discrepancy principle (DP) method [21] is adopted. The main idea of this method is to solve the functional equation

$$f(\alpha) = \left\|\mathbf{WJ}_\alpha^{(\delta)} - \mathbf{H}^{(\delta)}\right\|_2 - \|\boldsymbol{\delta}\|_2 = 0, \quad \alpha \geq 0. \quad (11)$$

Generally, finding $\alpha \geq 0$ such that $f(\alpha) = 0$ is a root finding problem, and the well-known Newton iteration method is used for the solution of (11).

While in most real world problems such good estimation of perturbation δ is not always available, therefore, it is necessary to employ alternative parameter selection strategy that avoids a knowledge of δ [22–24].

The first method is called L-curve criterion (LC) where α is chosen as the point with maximum curvature on the plot of $\log \|\mathbf{WJ}_{\text{reg}}^{(\delta)} - \mathbf{H}^{(\delta)}\|_2$ versus $\log \|\mathbf{LJ}_{\text{reg}}^{(\delta)}\|_2$. The overall shape of this plot typically has an L-shaped corner where the point with maximum curvature is located.

The second is generalized cross-validation (GCV) criterion. This method is to choose α by minimizing the GCV functional

$$G(\alpha) = \frac{\left\|\mathbf{WJ}_{\text{reg}}^{(\delta)} - \mathbf{H}^{(\delta)}\right\|_2}{\left(\text{trace}\left(\mathbf{I} - \mathbf{WR}_\alpha\right)\right)^2}. \quad (12)$$

The third method is quasi-optimality criterion (QO) and it is to minimize the functional equation

$$\begin{aligned} Q(\alpha) &= \alpha \left\| \frac{d\mathbf{J}_{\text{reg}}^{(\delta)}}{d\alpha} \right\|_2 \\ &= \left(\sum_i \left(f_i (1 - f_i) \frac{\mathbf{u}_i^T \mathbf{H}^{(\delta)}}{s_i} \right)^2 \right)^{1/2}, \end{aligned} \quad (13)$$

where $\mathbf{u}_i$ is the ith column of $\mathbf{U}$.

4. Numerical Results and Discussions

The approach is tested in four simulations with synthetic data. Figure 3 shows a flowchart of the simulation to study the performance of Tikhonov regularization complemented by four parameter selectors. Following [25], we use an exponential profile as the reference current density distribution $\mathbf{J}_{\text{ref}}$. The corresponding magnetic field reference is then calculated as $\mathbf{H}_{\text{ref}} = \mathbf{WJ}_{\text{ref}}$. Gaussian noise $\boldsymbol{\delta} := r \cdot \psi(\mathbf{H}_{\text{ref}})$ is generated by the synthetic noise generator with a signal-to-noise ratio of r^{-1} being superimposed onto $\mathbf{H}_{\text{ref}}$, yielding the perturbed reference of magnetic field $\mathbf{H}_{\text{ref}}{}^{(\delta)} = \mathbf{H}_{\text{ref}}{}^{(\delta)} + \boldsymbol{\delta}$. The function ψ produces a vector $\in \mathbb{R}^m$ of random entries with null average and standard deviation $\sigma = \|\mathbf{H}_{\text{ref}}\|_2 / \sqrt{m}$.

To evaluate the reconstructed solution, we define the relative errors on currents and magnetic fields in the 2-norm as

$$\begin{aligned} \varepsilon_J &:= \frac{\left\|\mathbf{J}_{\text{reg}} - \mathbf{J}_{\text{ref}}\right\|_2}{\left\|\mathbf{J}_{\text{ref}}\right\|_2}, \\ \varepsilon_H &:= \frac{\left\|\mathbf{H}_{\text{reg}} - \mathbf{H}_{\text{ref}}\right\|_2}{\left\|\mathbf{H}_{\text{ref}}\right\|_2}. \end{aligned} \quad (14)$$

The performance of parameter selectors and effects of signal-to-noise ratio, sensor number, and measurement distance on the performance are investigated in four simulations. We compute the mean value of relative errors on

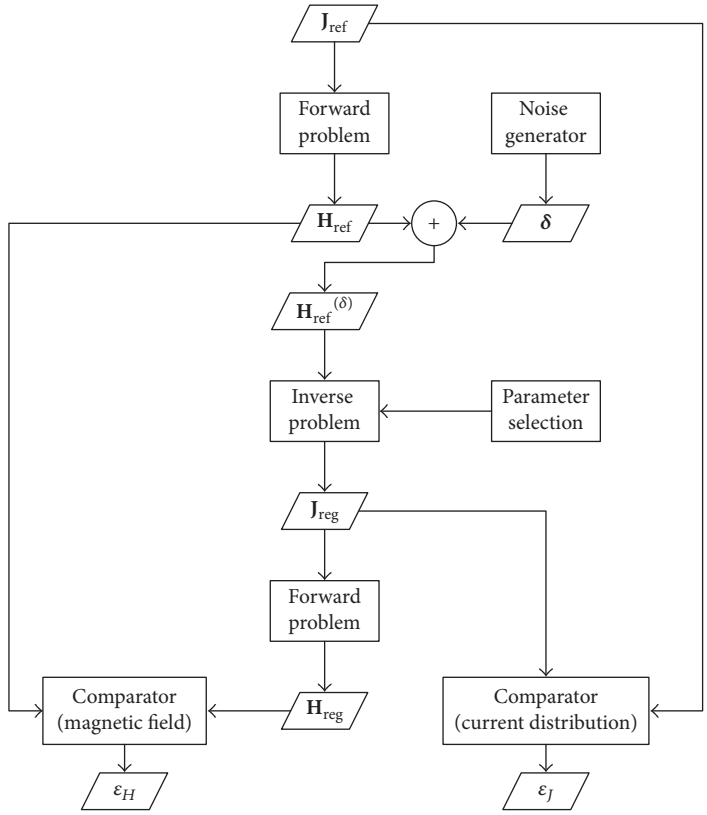

Figure 3: Flowchart of the simulation.

currents and magnetic fields for each simulation by using 100 realizations of randomly generated Gaussian noise.

Simulation I (Tikhonov regularization complemented by four parameter selectors). We set the discretization with levels $n_y = 80$, $n_z = 60$. We use a 16-by-16 measurement point matrix to perform magnetic measurements. The measurement distance x_d is set to be 10 mm. This set-up leads to the dimension of measurement space $m = 256$ and of current space $n = 4730$ with a spatial resolution of 0.5 mm; that is, the linear system of (6) is severely underdetermined. The case with $r = 10\%$ is considered. The reference of currents $\mathbf{J}_{\text{ref}}$ and the reconstruction results are shown in Figure 4. The plots of the L-curve, $G(\alpha)$, and $Q(\alpha)$ are shown in Figure 5. The optimized parameters and relative errors are listed in Table 1.

By employing the approach introduced in this work, we see a good agreement between the reference and reconstructed currents. The regularization scheme is observed to perform well. Moreover, the reference is reconstructed with a much smaller relative error on magnetic fields than that on currents; that is, $\mathbf{H}_1{}^{(\delta)}$ is reconstructed better than $\mathbf{J}_{\text{ref}}$. Similar results can also be seen in *Simulations I*, *II*, and *IV*, where $\mathcal{E}_H$ is always much larger than $\mathcal{E}_J$. This phenomenon shows the ill-posedness of the inverse problem in another way that even if the magnetic field has been reconstructed much more accurately, it is not guaranteed to obtain a much better reconstructed result of currents. Similar results have also been mentioned in [9].

Table 1: Parameters and relative errors in *Simulation I*.

Method	α	$\mathcal{E}_H$	$\mathcal{E}_J$
DP	1.9601×10^{-5}	1.3350×10^{-5}	5.3264×10^{-2}
GCV	6.5009×10^{-6}	3.0330×10^{-5}	4.9447×10^{-2}
LC	2.3840×10^{-6}	1.0893×10^{-5}	1.0255×10^{-1}
QO	1.5135×10^{-5}	1.1574×10^{-5}	4.9978×10^{-2}

The results in Figure 4 also show that errors are small over the nonarcing domain $\Omega_c \setminus \Omega_a$, where arc currents vanish, and the area of arc column. This result leads to a good approximation of the arc shape and location. Larger errors occur in the region of arc roots. In this test, we use a fixed mesh grid size; that is, the same grid size is used to operate the discretization of the continuous current distribution over the area of arc column and the area of arc roots. Because of the occurrence of a shrinkage phenomenon of arc domain profile near the arc roots region, which is usually the case in real arc plasmas, these fixed mesh grids are relatively rough. This means that the fixed mesh grid size is small enough for a particular spatial resolution of the method but is too large to approximate the current distribution in the area of arc roots. Another very important reason for this phenomenon is the

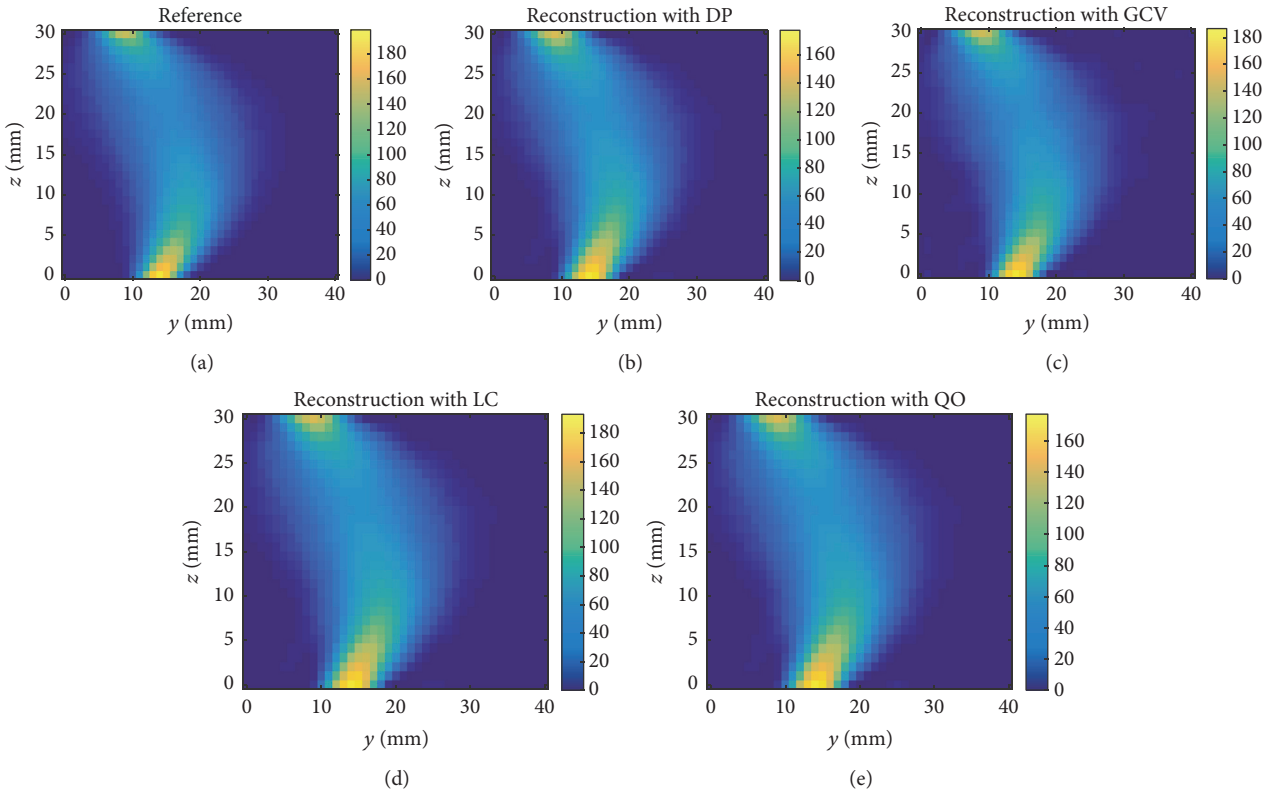

FIGURE 4: *Simulation I*. The reference of currents (at (a)) and the reconstruction of currents with four parameter selection criteria: discrepancy principle method (b), generalized cross-validation (c), L-curve criterion (d), and quasi-optimality criterion (e).

error in estimation of root locations, which results in a larger error in this region.

The parameter selector of LC is observed to perform much worse than DP, GCV, and QO with a larger relative error on current of more than 10% and larger distortions are seen in Figure 4, while DP, GCV, and QO behave more or less the same. The functions of $G(\alpha)$ and $Q(\alpha)$ in Figure 5 are seen to be changing smoothly versus α and no local minimums are observed in the range of α investigated which guarantees a good performance when choosing α by minimizing the GCV and QO functional.

Simulation II (sensitivity to noise level). The robustness and tolerance of these four parameter selection criteria are studied in this test. The question arises as to the maximal accuracy attainable given the level of SNR in the measurement data. In this case, the set-up of measurement surface and of sensor array are set to be the same as used in *Simulation I*. But the method is tested with different values of r to assess the sensitivity to SNR. Figure 6 shows the mean values of relative error on magnetic fields and on currents versus r with different criterion. In the explored range of r (10^{-10}~10^{-1}), the logarithm of mean values of relative error on magnetic fields is observed to decrease linearly with the decrement of the logarithm of r for the four parameter selectors. And $\mathcal{E}_H$ is limited to 1% when r is no larger than 10^{-1}. The similar tendency can also be seen in $\mathcal{E}_J$ except that when the LC criterion is used, $\mathcal{E}_J$ is increasing with the decrement of r.

The DP, GCV, and QO criteria are observed to behave more or less the same versus the explored range of noise ratios. The LC criterion fails in reconstruction of the current distribution, although its performance on the reconstruction of magnetic fields is seen to be approximately the same as the other three. Large relative errors on currents and instability are observed from Figure 6. However, the DP criterion can only be used if a good estimation of measurement perturbations is known, while that is usually impossible in practical applications. Therefore, GCV and QO criteria seemed to be more attractive when optimizing the regularization parameter for this kind of magnetic inverse problems.

Simulation III (sensitivity to sensor number). The effect of the dimension of measurement space is analyzed in this test. The set-up of the measurement surface and the sensor array used in *Simulation I* is replaced by an array $|P_y|$-by-$|P_z|$, where $|P_y| = \chi \cdot n_y$, $|P_z| = \chi \cdot n_z$ with the parameter $\chi \in \{0.1, 0.2, 0.5, 0.7, 0.9, 1.0, 1.1, 1.2, 1.5, 2.0\}$. Figure 7 shows the relative errors on magnetic fields and on currents versus the dimensional ratio which is defined by $\dim_r = m/n = \chi^2$. Then the linear problem of (6) is underdetermined, square, or overdetermined when $\dim_r <, =, > 1$, respectively.

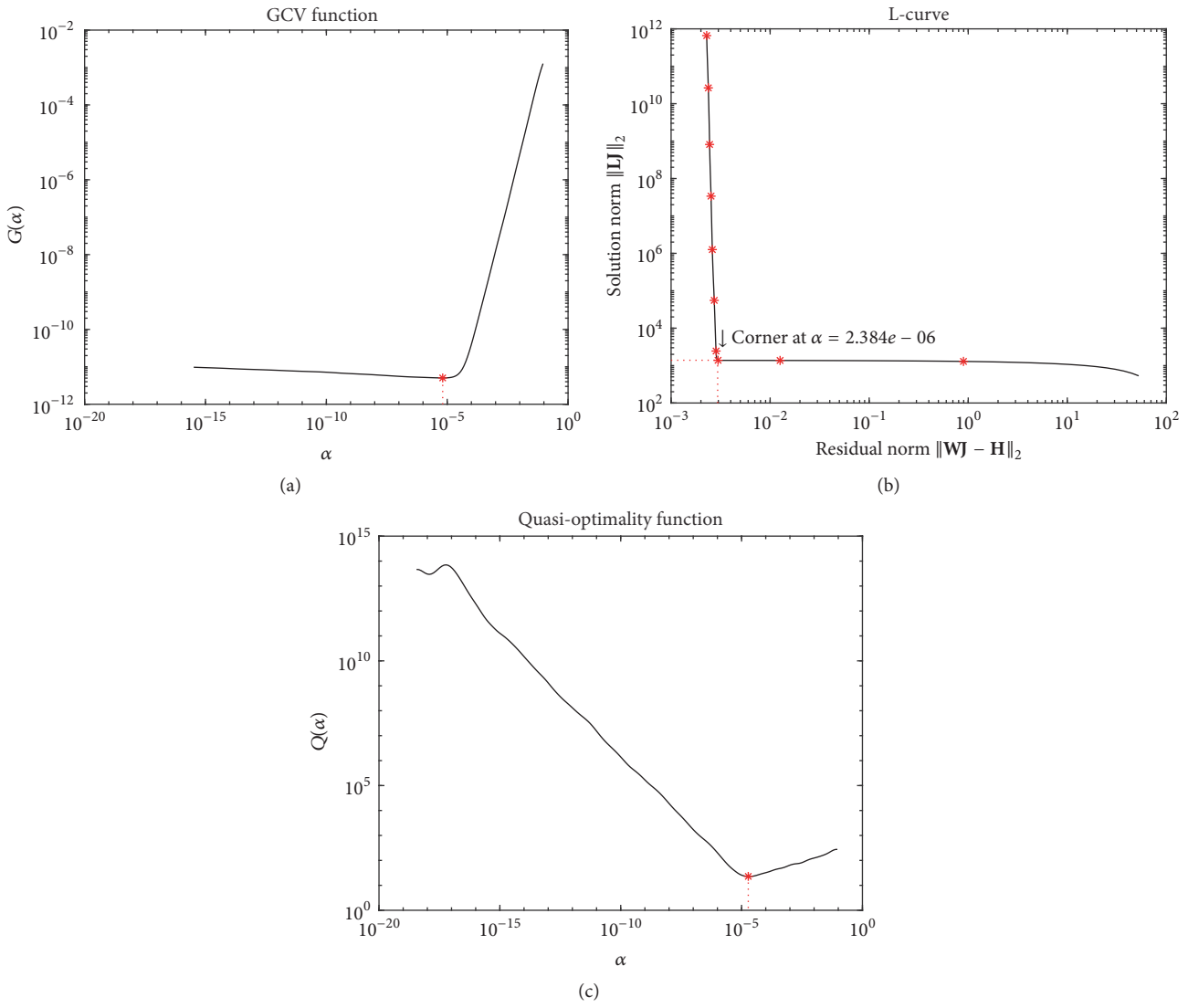

FIGURE 5: *Simulation I*. Plot of $G(\alpha)$ versus α (a), plot of $\log \|\mathbf{WJ}_\alpha{}^{(\delta)} - \mathbf{H}^{(\delta)}\|_2$ versus $\log \|\mathbf{LJ}_\alpha{}^{(\delta)}\|_2$ (b), and the $G(\alpha)$ curve versus (c). The minimal points of $G(\alpha)$ and of $Q(\alpha)$ are marked out with the red asterisk.

The mean values of relative error on currents are observed to decrease with the increment of $\dim_r$ for the range of $\dim_r \leq 1$. The rate of decrement in $\mathcal{E}_J$ with these four parameter selection methods is approximately the same. Furthermore, for the range of $\dim_r > 1$, $\mathcal{E}_J$ stays around a value of about 1%. The increasing number of magnetic sensors leads to a transformation of the problem in (6), from the underdetermined pattern to the overdetermined pattern. A larger number of magnetic sensors result in a better reconstruction performance of the current density distribution for the underdetermined linear problem of (6) but are observed to have less influence on the overdetermined pattern. In other words, if we desire to achieve a higher spatial resolution of current density distribution, we are supposed to put more sensors on measurement surface until the system is overdetermined. But larger number of sensors can make the set-up system too complex to handle with, so one has to make a compromise between the complexity of the system with the reconstruction accuracy and spatial resolution.

The similar results can also be observed in the reconstructed magnetic fields. An exception is seen in $\mathcal{E}_H$ with GCV method for the range of $\dim_r \leq 1$, where the increasing number of sensors leads to a worse result of magnetic fields reconstruction. But the level of $\mathcal{E}_H$ is limited to 10^{-4} which is still a satisfactory result.

Another point we should take care of is that the LC criterion performs much worse than the other three criteria no matter what the value of dimensional ratio is.

Simulation IV (sensitivity to measurement distance). The effect of measurement distance is analyzed in this test. In this case, the set-up of the measurement surface boundary

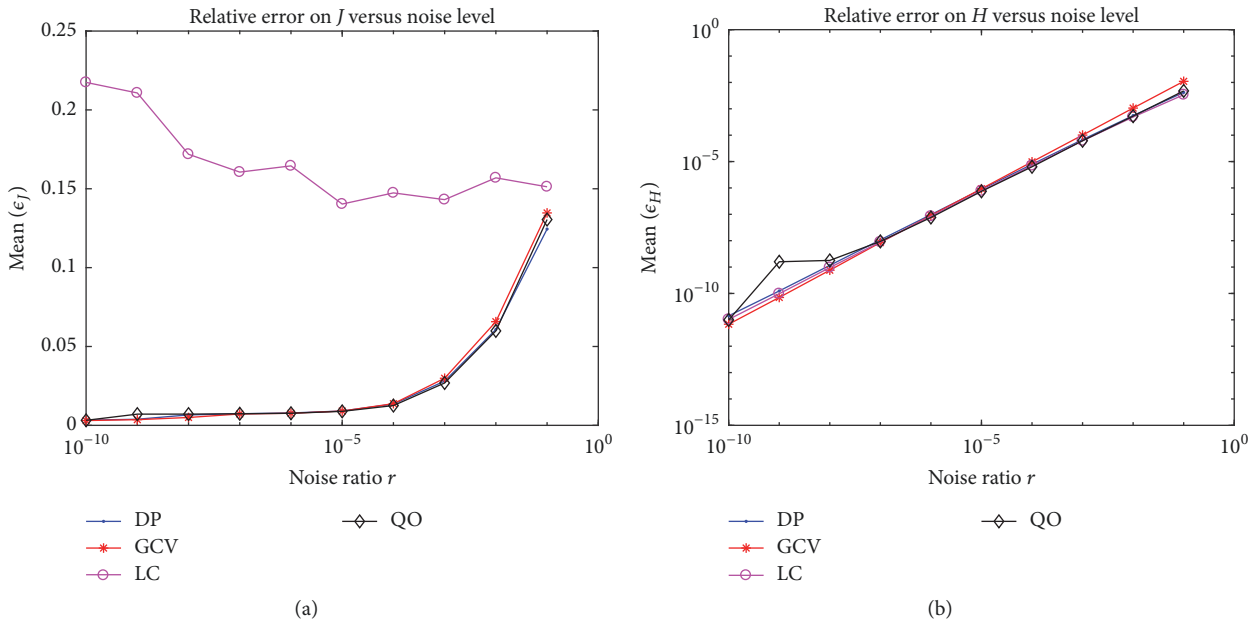

FIGURE 6: *Simulation II*. Mean values of relative error on currents (a) and on magnetic fields (b) versus noise ratio r with four parameter selection criteria. The mean values are computed in 100 repeated runs for each value of noise ratio r with the noise generator randomly producing Gaussian noise.

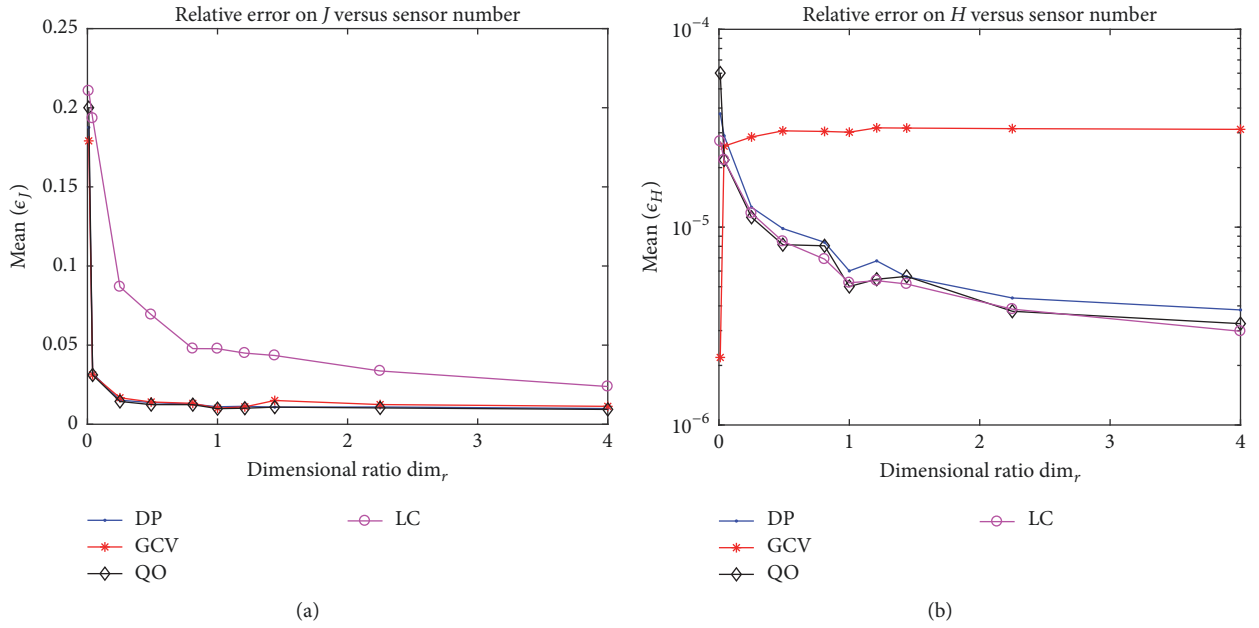

FIGURE 7: *Simulation III*. Mean values of relative error on currents (a) and on magnetic fields (b) versus dimensional ratio dim$_r$ with four parameter selection criteria. The mean values are computed in 100 repeated runs for each value of dimensional ratio dim$_r$.

and the set-up of the sensor array are the same as that used in *Simulation I* and measurement distance is set to be $x_d \in \{1\,\text{mm}, 2\,\text{mm}, \ldots, 30\,\text{mm}\}$. The results are shown in Figure 8.

Some U-shape curves are observed in the results achieved with DP, GCV, and QO criteria. Larger relative errors in the solution will be met when the sensor arrays are located too close to or too far away from the test object. An optimal value of x_d can be seen in the range of $5\,\text{mm} \leq x_d \leq 15\,\text{mm}$ for the studied geometry model in this work. The mean values of relative errors on currents achieved by the LC criterion are much larger than that by the other three criteria and no optimal measurement distance can be observed.

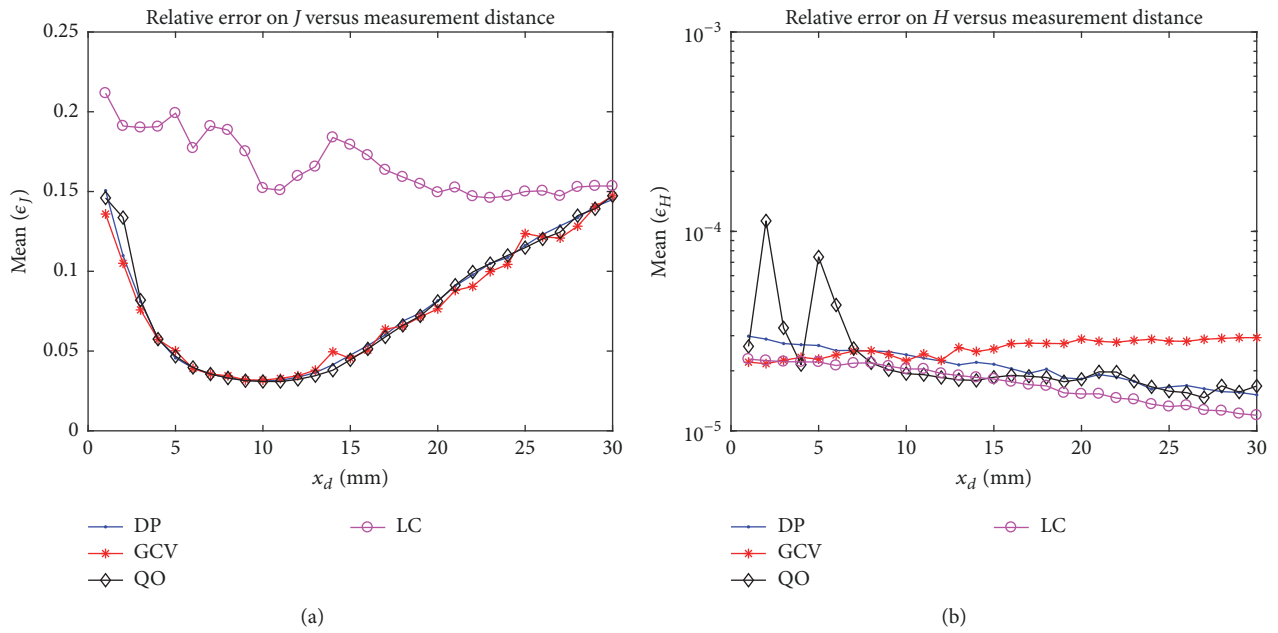

FIGURE 8: *Simulation IV*. Mean values of relative error on currents (a) and on magnetic fields (b) versus measurement distance x_d with four parameter selection criteria. The mean values are computed in 100 repeated runs for each value of measurement distance x_d.

The magnetic field H defined in (1) is uniquely determined by the trace of H on the boundary ∂G of some domain G with $\overline{\Omega} \in G$ [3]. Generally, the better the knowledge about the external magnetic field is, which usually demands more measurement points (larger number of sensors), the better the accuracy of the solution can be expected. But in most practical applications, it is impossible to measure the whole magnetic field. Magnetic measurements are usually obtained by sensor arrays, spatially. The number of sensors is often limited by physical geometries and economic constraints (hardware and software costs). Only parts of H are measured by a limited number of sensors of an array. In particular, when a planner array of sensors is used, the magnetic field over the measurement plane Γ is measured whose spatial resolution is determined by the number of measurement points. We denote the cross product in (1) with a measurement distance x_d by

$$\begin{pmatrix} \tau_x \\ \tau_y \\ \tau_z \end{pmatrix} = \begin{pmatrix} J_x \\ J_y \\ J_z \end{pmatrix} \times \begin{pmatrix} x - x_d \\ y - y_s \\ z - z_s \end{pmatrix} = \begin{pmatrix} J_y (z - z_s) - J_z (y - y_s) \\ J_z (x - x_d) - J_x (z - z_s) \\ J_x (y - y_s) - J_y (x - x_d) \end{pmatrix}. \tag{15}$$

For any integration point r_s in source space, the contribution of x-component H_x to the whole magnetic field H at measurement point r is computed with

$$\frac{\left(J_y (z - z_s) - J_z (y - y_s)\right)^2}{\left(\left(J_y (z - z_s) - J_z (y - y_s)\right)^2 + \left(J_z (x - x_d) - J_x (z - z_s)\right)^2 + \left(J_x (y - y_s) - J_y (x - x_d)\right)^2\right)^2}. \tag{16}$$

By taking the integration for source space Ω in (1), we see that, from (15), the contribution of H_x to H is decreasing with the increment of x_d. Thus, we obtain less information about the whole magnetic field when the measurement distance is larger, leading to a worse solution with larger errors as shown in Figure 8 in the investigated range of $x_d \leq 5$ mm. Meanwhile, as we can see in (1), the magnitude of magnetic field H is also decreasing with the increment of x_d. When x_d is too large, the magnetic field becomes very weak. In practical applications, the magnetic sensors with a certain sensitivity can detect nothing but environmental noises. The proportion of perturbations in the measurement data H_{meas} becomes larger, and then larger relative errors are observed due to the illness of the inverse problem as shown in Figure 8 in the investigated range of $x_d \geq 15$ mm. So an optimal value of the measurement distance x_d can be expected when we are using a planner sensor array to perform magnetic measurements, which is related to the signal-to-noise ratio and the area of the measurement plane.

5. Conclusion

An approach to reconstruct the current density distribution in electric arc plasmas inside LVCBs by inverting the magnetic fields has been proposed. This method is tested with a 2D arc model in a simplified chamber. The Tikhonov regularized least squares solution, complemented by four criteria for the choice of regularization parameter, shows good spatial resolution and numerical accuracy under severe perturbations of magnetic fields. In the provided range of regularization parameter selectors, the DP, GCV, and QO criteria behave more or less the same for the optimization of parameter with the Tikhonov regularization when regularizing the magnetostatic inverse problem of current distribution reconstructions for LVCBs, while we conclude that the GCV and QO criteria are observed to be the more attractive methods with satisfactory performance considering the situation where in most practical applications such a good estimation of perturbations, which is indispensable for the DP criterion, is not always accessible. The method presented is observed to have a good quality of robustness as seen in *Simulation II*. A larger number of sensors are seen to improve the quality of the reconstructed results significantly for underdetermined systems but have little influence for square and overdetermined systems *(Simulation III)*. When using a planner array of magnetic sensors, an optimal measurement distance can be expected (a range of $5\,\text{mm} \leq x_d \leq 15\,\text{mm}$ for the studied geometry model in *Simulation IV*).

The nature of this approach is that of the feasibility and convenience to operate the estimation of current density distribution with a given geometry structure of LVCB and to set up a LVCB under test. The approach presented in this study could be used to accomplish the computational side of the inverse problem and to identify the experimental data.

Conflicts of Interest

The authors declare that there are no conflicts of interest regarding the publication of this paper.

Acknowledgments

This work was supported by the National Natural Science Foundation of China under Grant 51477129.

References

[1] P. Freton and J. Gonzalez, "Overview of current research into low-voltage circuit breakers," *The Open Plasma Physics Journal*, vol. 2, no. 2, pp. 105–119, 2009.

[2] F. Yang, Y. Wu, M. Rong et al., "Low-voltage circuit breaker arcs—simulation and measurements," *Journal of Physics D: Applied Physics*, vol. 46, no. 27, Article ID 273001, 2013.

[3] R. Kress, L. Kühn, and R. Potthast, "Reconstruction of a current distribution from its magnetic field," *Inverse Problems*, vol. 18, no. 4, pp. 1127–1146, 2002.

[4] M. Le Ny, O. Chadebec, G. Cauffet et al., "Current distribution identification in fuel cell stacks from external magnetic field measurements," *IEEE Transactions on Magnetics*, vol. 49, no. 5, pp. 1925–1928, 2013.

[5] O. A. Shyshkin, Y. G. Kazarinov, M. Tallouli, T. Famakinwa, and S. Yamaguchi, "Inverse problem solution algorithms for current density distribution calculation in different HTS tape configurations basing on minimum self-magnetic field measurements," *IEEE Transactions on Applied Superconductivity*, vol. 26, no. 3, Article ID 9000404, 2016.

[6] J. Jang, C. Y. Ahn, J.-I. Choi, and J. K. Seo, "Inverse problem for color doppler ultrasound-assisted intracardiac blood flow imaging," *Computational and Mathematical Methods in Medicine*, vol. 2016, Article ID 6371078, pp. 1–10, 2016.

[7] C. J. S. Alves, R. Mamud, N. F. M. Martins, and N. C. Roberty, "On inverse problems for characteristic sources in Helmholtz equations," *Mathematical Problems in Engineering*, vol. 2017, Article ID 2472060, pp. 1–16, 2017.

[8] J.-P. Toumazet, C. Brdys, A. Laurent, and J.-L. Ponthenier, "Combined use of an inverse method and a voltage measurement: estimation of the arc column volume and its variations," *Measurement Science and Technology*, vol. 16, no. 7, pp. 1525–1533, 2005.

[9] L. Ghezzi, D. Piva, and L. Di Rienzo, "Current density reconstruction in vacuum arcs by inverting magnetic field data," *IEEE Transactions on Magnetics*, vol. 48, no. 8, pp. 2324–2333, 2012.

[10] J. Dong, G. Zhang, Y. Geng, and J. Wang, "Current distribution reconstruction in switching air arcs by inverting external magnetic fields," in *Proceedings of the ICEF 2016, 7th International Conference Electromagnetic field problems and Applications*, Xi'an, China, Septemper 2016.

[11] J. Dong, G. Zhang, Y. Geng, and J. Wang, "Influence of magnetic measurement modeling on the solution of magnetostatic inverse problems applied to current distribution reconstruction in switching air arcs," in *Proceedings of the 21th International Conference on the Computation of Electromagnetic Field (COMPUMAG '17)*, Daejeon, Korea, June 2017.

[12] Y. Fei, R. Mingzhe, W. Yi et al., "Numerical simulation of the eddy current effects on the arc splitting process," *Plasma Science and Technology*, vol. 14, no. 11, pp. 974–979, 2012.

[13] A. Iturregi, B. Barbu, E. Torres, F. Berger, and I. Zamora, "Electric arc in low-voltage circuit breakers: experiments and simulation," *IEEE Transactions on Plasma Sciences*, vol. 45, no. 1, pp. 113–120, 2017.

[14] C. Brdys, J. P. Toumazet, A. Laurent, and J. L. Ponthenier, "Optical and magnetic diagnostics of the electric arc dynamics in a low voltage circuit breaker," *Measurement Science and Technology*, vol. 13, no. 7, pp. 1146–1153, 2002.

[15] B. Kubicek and K. A. Berger, "Modeling moving electric arcs: verification of a coupled fluid-dynamics magnetostatic approach," *IEEE Transactions on Magnetics*, vol. 44, no. 6, pp. 790–793, 2008.

[16] J.-P. Toumazet, C. Brdys, A. Laurent, and J.-L. Ponthenier, "Experimental study of breaking devices arcs using coupled optical and magnetic measurements," *IEEE Transactions on Plasma Sciences*, vol. 36, no. 4, pp. 1036-1037, 2008.

[17] J. W. McBride, A. Balestrero, L. Ghezzi, G. Tribulato, and K. J. Cross, "Optical fiber imaging for high speed plasma motion diagnostics: applied to low voltage circuit breakers," *Review of Scientific Instruments*, vol. 81, no. 5, Article ID 055109, 2010.

[18] R. Potthast and L. Kühn, "On the convergence of the finite integration technique for the anisotropic boundary value problem of magnetic tomography," *Mathematical Methods in the Applied Sciences*, vol. 26, no. 9, pp. 739–757, 2003.

[19] G. Lehner, *Electromagnetic Field Theory for Engineers and Physicists*, Springer, Dordrecht, Netherlands, 2010.

[20] K.-H. Hauer, R. Potthast, and M. Wannert, "Algorithms for magnetic tomography—on the role of a priori knowledge and constraints," *Inverse Problems*, vol. 24, no. 4, Article ID 045008, 2008.

[21] L. Rondot, O. Chadebec, and G. Meunier, "3-D magnetostatic moment method dedicated to arc interruption process modeling," *IEEE Transactions on Magnetics*, vol. 50, no. 2, 2014.

[22] H. W. Engl, M. Hanke, and A. Neubauer, *Regularization of Inverse Problems*, Kluwer Academic, Dordrecht, Netherlands, 1996.

[23] A. Dienstfrey and P. D. Hale, "Colored noise and regularization parameter selection for waveform metrology," *IEEE Transactions on Instrumentation and Measurement*, vol. 63, no. 7, pp. 1769–1778, 2014.

[24] R. Bortel and P. Sovka, "Regularization techniques in realistic Laplacian computation," *IEEE Transactions on Biomedical Engineering*, vol. 54, no. 11, pp. 1993–1999, 2007.

[25] B. Swierczynski, J. J. Gonzalez, P. Teulet, P. Freton, and A. Gleizes, "Advances in low-voltage circuit breaker modelling," *Journal of Physics D: Applied Physics*, vol. 37, no. 4, pp. 595–609, 2004.